AGU ADVANCING EARTH AND SPACE SCIENCE

Geophysical Research Letters

RESEARCH LETTER
10.1029/2021GL093231

On the Relevance of Geodetic Deformation Rates to Earthquake Potential

Kelin Wang[1,2], Yijie Zhu[2], Edwin Nissen[2], and Zheng-Kang Shen[3]

[1]Pacific Geoscience Centre, Geological Survey of Canada, Sidney, BC, Canada, [2]School of Earth and Ocean Sciences, University of Victoria, Victoria, BC, Canada, [3]Department of Earth, Planetary, and Space Sciences, University of California, Los Angeles, CA, USA

Key Points:

- Because of viscoelasticity, faults with long recurrence intervals accrue most of their elastic strain early in the interseismic period
- Strain rates should not be conflated with stored strain, and slow geodetic deformation rates do not imply limited earthquake potential
- For strike-slip faults, "Relative Displacement Deficit" is a better measure of the earthquake readiness of a fault than "slip deficit"

Supporting Information:

Supporting Information may be found in the online version of this article.

Correspondence to:

K. Wang,
kelin.wang@canada.ca

Citation:

Wang, K., Zhu, Y., Nissen, E., & Shen, Z.-K. (2021). On the relevance of geodetic deformation rates to earthquake potential. *Geophysical Research Letters*, *48*, e2021GL093231. https://doi.org/10.1029/2021GL093231

Received 4 MAR 2021
Accepted 21 APR 2021

Abstract Despite the importance of viscoelasticity in the evolution of crustal stress/strain being widely recognized, the interpretation of interseismic geodetic measurements for assessing earthquake potential is still based overwhelmingly on elastic models. The reasons for this disparity include conflating deformation rates with deformation itself and the lack of a succinct representation of the seismic readiness of a locked fault in a viscoelastic Earth. Using a classical viscoelastic model for strike-slip faults, we reiterate the commonly overlooked message that, if the recurrence interval is long, most of the strain energy for the next earthquake accrues early in the cycle, and low strain rates later in the cycle by no means indicate diminished rupture potential. Fault stress stays near failure for much of the late interseismic period which may explain why slow slip-rate faults have more variable recurrence intervals than fast slip-rate faults. We propose to use displacement deficit instead of slip deficit to represent seismic readiness.

Plain Language Summary Modern satellite measurements can reveal how quickly faults are being loaded by tectonic plate motions, and seismic hazard models use these loading rates as proxy for the likelihood of a pending earthquake. However, because of the partially fluid-like behavior of Earth's interior, these loading rates have actually evolved with time since the last rupture. For faults with long intervals between successive earthquakes, these rates slow down substantially as the next event draws near. We, therefore, caution that slow rates of loading should not be assumed to reflect limited earthquake potential.

1. Introduction

Geodetic measurements of crustal deformation complement earthquake records and paleoseismic evidence in the evaluation of the seismic potential of locked faults. However, because geodetic measurements only constrain strain rate but not the accumulated strain that will propel the next earthquake, their relevance to seismic potential is questionable.

A link between deformation rates and seismic potential can be made if interseismic deformation is modeled assuming an elastic Earth. For example, in the elastic dislocation model of a locked strike-slip fault (Savage & Burford, 1973; Figure 1a), fault-parallel velocity $V(x)$ at the surface, being constant with time $t(>0)$ from the last earthquake (Figure 1b), is a scaled mirror image of coseismic deformation (Figure 1c). Because displacement $U(x,t)=V(x)t$, the seismic readiness of the fault for the next earthquake can be characterized by its slip deficit $S = V_o t$, where V_o is the geological slip rate of the fault (Figure 1a). At the end of an earthquake cycle $t = T$, S reaches its theoretical maximum $U_o = V_o T$, and the fault is fully ready for an earthquake. The same applies to the thrust fault model shown in Figure S1a (Savage, 1983).

It is now beyond any doubt that the Earth exhibits viscoelasticity in earthquake cycles (e.g., Chuang & Johnson, 2011; Hearn & Thatcher, 2015; Johnson, 2013; Meade et al., 2013; Takeuchi & Fialko, 2012; K. Wang et al., 2012; Zhu et al., 2020). In a viscoelastic Earth, the deformation rate changes with time throughout the interseismic period so that the interseismic velocity pattern may not resemble a mirror image of coseismic deformation, and the slip deficit S may not be an appropriate metric of seismic readiness. However, despite broad applications of viscoelastic models in interpreting postseismic deformation, the interpretation of interseismic deformation for earthquake potential is still based overwhelmingly on concepts derived from elastic models as outlined in the preceding paragraph.

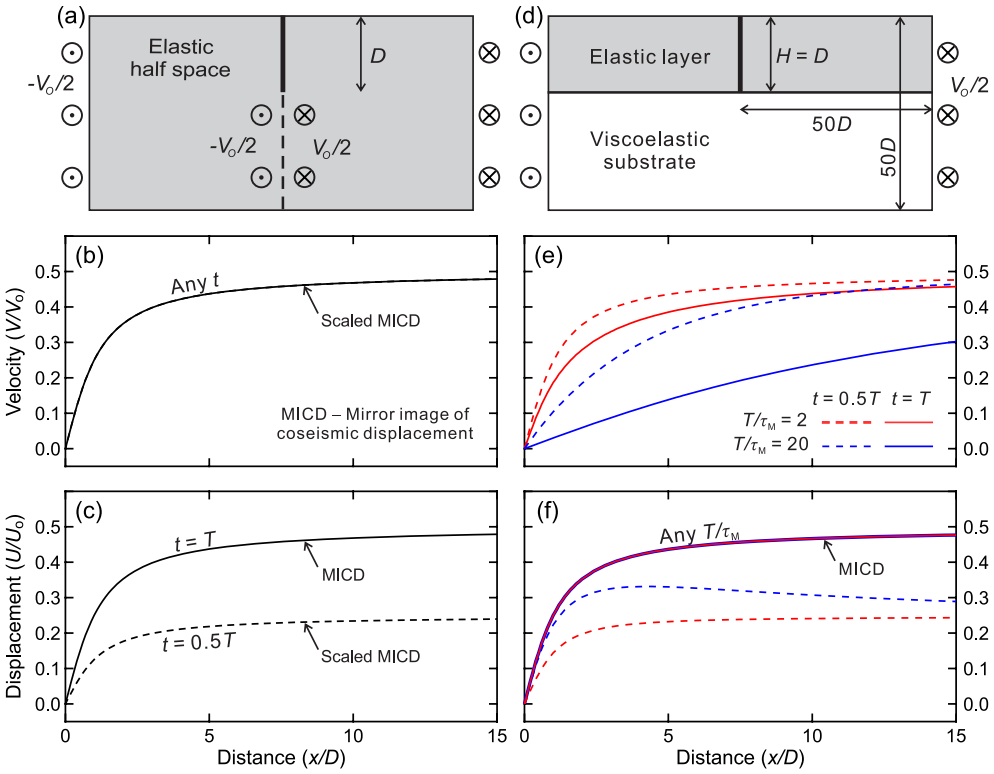

Figure 1. Two-dimensional earthquake-cycle models for a vertical strike-slip fault with geological slip rate V_o and periodic earthquakes at interval T with slip $U_o = V_oT$. (a) Elastic dislocation model (not to scale). (b) Fault-parallel surface velocity from the model in (a). (c) Similar to (b) but for surface displacements at the mid- and late-interseismic stages. (d) Viscoelastic model (not to scale). Shown model dimensions are for the finite element modeling in this work. (e) Fault-parallel surface velocity from the model in (d) at two interseismic stages for two different values of T/τ_M. (f) Similar to (e) but for surface displacements. Displacements at $t = T$ are the same for any value of T/τ_M and identical to that in (c).

We think that the peculiar tenacity of elastic models is due to two primary reasons. The first reason is a conflation of deformation rate with deformation itself by researchers; geodetic velocities and strain rates are somehow thought to represent the strain required by future seismic rupture. The second reason is the absence of a succinct alternative to the slip deficit concept to quantify the seismic readiness of faults in viscoelastic models. There are other minor reasons such as the similarity between viscoelastic and elastic models in the case of short recurrence intervals (Zhu et al., 2020) and the convenience of inverting geodetic data to infer fault locking state using elastic models. In this study, we address the two primary reasons by revisiting a classical viscoelastic earthquake-cycle model that is comparable to the dislocation model in Figure 1a in terms of simplicity. We reiterate the commonly overlooked message that, if the earthquake recurrence interval is long or if the viscosity beneath the elastic layer is low, deformation rates become very low toward the end of the interseismic period, but these low rates by no means lessen the fault's ability to produce a large earthquake soon. We also propose a new term, the Relative Displacement Deficit (RDD), as a better alternative to slip deficit.

2. Earthquake Cycles in a Viscoelastic Earth

2.1. Velocity Versus Displacement

Shown in Figure 1d is the classical viscoelastic earthquake-cycle model for a strike-slip fault featuring an elastic plate of thickness H overlying a uniform Maxwell viscoelastic half space with viscosity η_M. Although analytical solutions are available (Nur & Mavko, 1974; Savage & Prescott, 1978), we use a numerical (finite element) version with dimensions shown in Figure 1d for the ease of explicitly applying boundary loading

conditions. A similar model for a thrust fault is shown in Figure S1d. The Maxwell relaxation time of the substrate is $\tau_M = \eta_M/\mu$, where μ is rigidity which is assumed to be uniform in the model. For μ = 31.7 GPa and $\eta_M = 5 \times 10^{19}$ Pa s, τ_M = 50 years. The Poisson's ratio is assumed to be 0.25 uniformly. The symmetric system is driven from the far-field boundaries by a constant velocity $\pm 0.5V_o$. The fault (at $x = 0$) is locked from the surface to depth D but ruptures the same depth range at recurrence interval T with coseismic slip $U_o = V_oT$. Despite the simplifying assumptions such as $D = H$ and T being constant for the sake of mathematical convenience, the physical insights communicated by this model apply to more realistic situations. For details of the modeling procedure, three-dimensional effects, and/or more complex rupture histories see Zhu et al. (2020).

In contrast to the elastic model, surface velocity in the viscoelastic model is not constant with time (Figure 1e), and surface displacement is not a linear function of time (Figure 1f). The deformation field depends on the ratio T/τ_M. For understanding the effect of rheology, it is convenient to imagine a constant T and examine how the deformation is affected by τ_M. To connect to real faults, it is usually more useful to imagine a constant τ_M and examine how the evolution of deformation differs between different lengths of T.

If T is long or τ_M is small, the velocities are much lower later in the cycle (Figure 1e, blue solid line), but more displacement is accrued earlier in the cycle (Figure 1f, blue dashed line). The earthquake-cycle model for a thrust fault shows the same behavior but in terms of fault-normal velocities and displacements (Figures S1e and S1f). Because of cycle-invariance, the displacement at the end of the cycle $U\left(x,T\right)$ is a mirror image of coseismic displacement (Figure 1f). Because coseismic deformation is elastic and hence identical to that of the elastic dislocation model, $U\left(x,T\right)$ in Figure 1f is also identical to that in Figure 1c, independent of T/τ_M. This "final" displacement distribution has the familiar arctan shape:

$$U\left(x,T\right) = \frac{U_o}{\pi}\arctan\frac{x}{D} \tag{1}$$

The rheological structure shown in Figure 1d is the simplest possible with the fewest parameters for the purpose of this study. It is ideal for our purpose because it is the most conservative in illustrating the viscoelastic effect in a two-dimensional (2-D) setting. The viscoelastic effect is more pronounced for greater T/τ_M. Although Equation 1 always holds, adding other rheological complexities, such as transient rheology, nonlinear rheology, and a velocity-strengthening segment or low-viscosity shear zone below the brittle fault, will hasten stress relaxation early in the interseismic period. The effect is qualitatively similar to reducing τ_M and hence makes the viscoelastic effect even stronger. The performance of some of these more complex models in terms of deformation rates can be seen in the work of Zhu et al. (2020).

2.2. Strain/Stress Rate Versus Strain/Stress

It is convenient to use the following normalized engineering shear strain rate $\dot{\Gamma}_o$ at the surface and at the fault trace (the slope of the velocity curve at $x = 0$ in Figure 1e) to represent the rate of energy buildup toward the next earthquake,

$$\dot{\Gamma}_o\left(t\right) = \frac{D}{V_o}\frac{\partial V}{\partial x} \tag{2}$$

The corresponding normalized shear strain (the slope of the displacement curve at $x = 0$ in Figure 1f) is

$$\Gamma_o\left(t\right) = \frac{D}{U_o}\frac{\partial U}{\partial x} \tag{3}$$

The evolution of $\dot{\Gamma}_o$ and Γ_o in an earthquake cycle for selected T/τ_M ratios is shown in Figures 2a and 2b, respectively, in comparison with elastic model predictions. Their dependency on T/τ_M is illustrated in Figures 2c and 2d for selected time points. The maximum value of Γ_o is π^{-1} and occurs at the end of the cycle. It is independent of T/τ_M and can be determined from Equation 1. For smaller T/τ_M, the interseismic strain and its rate are more similar to those of the elastic model. However, the longer the recurrence interval (or the lower the viscosity), the more strain is accrued earlier in the cycle, making up the "deficiency" due to

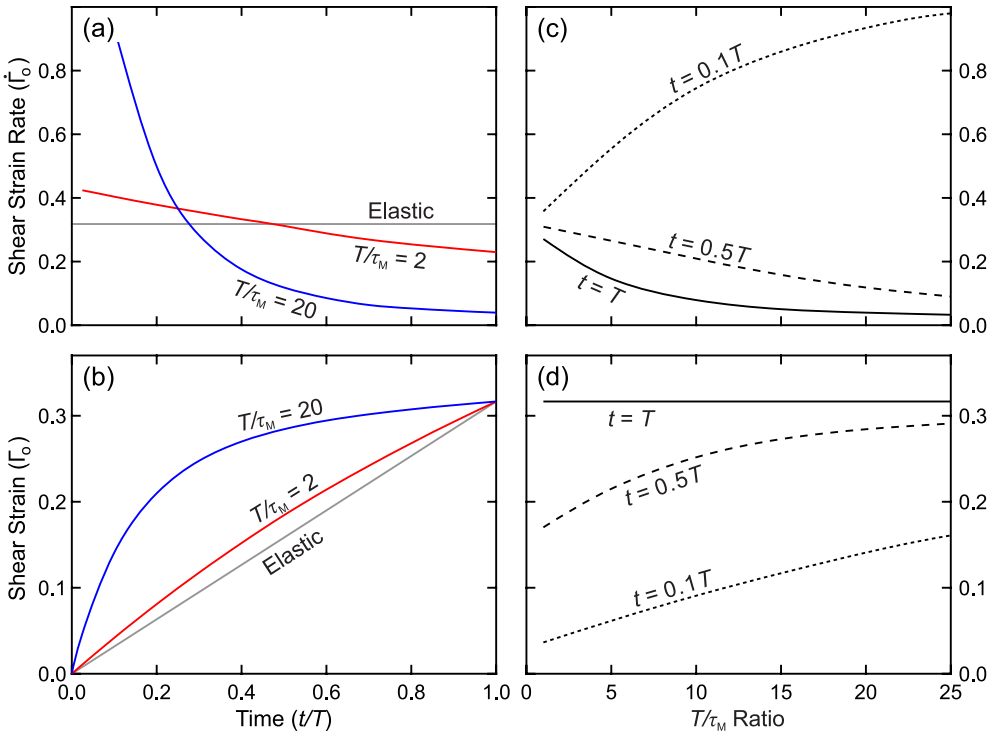

Figure 2. Normalized shear strain Γ_o since the last earthquake or its rate $\dot{\Gamma}_o$ (Equations 3 and 2, respectively) at $x = 0$ in the model shown in Figure 1d. Stress or its rate is obtained by multiplying Γ_o with $\mu U_o/D$ or $\dot{\Gamma}_o$ with $\mu V_o/D$, respectively. (a) and (b) Evolution of $\dot{\Gamma}_o$ and Γ_o, respectively, in an earthquake cycle. Predictions of the elastic model (Figure 1a) are shown for comparison. (c) and (d) $\dot{\Gamma}_o$ and Γ_o, respectively, at three interseismic time points for different T/τ_M ratios. At $t = T$, $\Gamma_o = \pi^{-1}$, the same as in the elastic model and independent of T/τ_M, as is also obvious in (b).

slower deformation later in the cycle. For a dipping thrust fault, the relevant metrics are fault-normal normal strain and its rate averaged over a distance interval. For an averaging interval 0–5D, the normal strain Ω_{5D} and its rate $\dot{\Omega}_{5D}$ are shown in Figures S2. They show the same behavior as Γ_o and $\dot{\Gamma}_o$.

Multiplying $\Gamma_o U_o/D$ or $\dot{\Gamma}_o V_o/D$ with μ gives the incremental shear stress or its rate of increase, respectively, at time t since the last earthquake. For example, for $U_o = 10$ m, $D = 20$ km, and $\mu = 31.7$ GPa, the maximum Γ_o represents an incremental shear stress about 5 MPa, comparable to commonly observed values of earthquake stress drop.

The strain (or stress) depicts the elastic strain energy already stored in the system and is what matters to the next earthquake. Given viscosity, for long recurrence intervals, most of the stress buildup occurs earlier in the interseismic period. When the stress is high enough to drive the fault to failure, its rate of increase can be very low. Therefore, geodetically observed low rates of deformation do not necessarily indicate lower likelihood of a pending earthquake. The idealized models in Figures 1d–1f (or S1d–S1f) and Figure 2 (or S2) show the opposite: For a locked large fault with a long recurrence interval, lower deformation rates (normalized by V_o) signal greater immediacy of the next earthquake.

2.3. Slip Deficit Versus Displacement Deficit

As mentioned in the Introduction, slip deficit $S = V_o t$ as a measure of seismic readiness is based on the assumption of an elastic Earth in which strain energy accumulates linearly with time. For example, if the present time is $t = 0.5T$, then $S = 0.5U_o$. Viewed in a "slip-predictable" framework (Shimazaki & Nakata, 1980), the fault is ready for a seismic slip $0.5U_o$. Viewed in a "time-predictable" framework (Shimazaki & Nakata, 1980), the fault needs to build up slip deficit for another $0.5T$ to prepare for a seismic slip U_o. Figure 2 (or S2) serves to remind us that in a viscoelastic Earth the accumulation of strain energy is not linear with time.

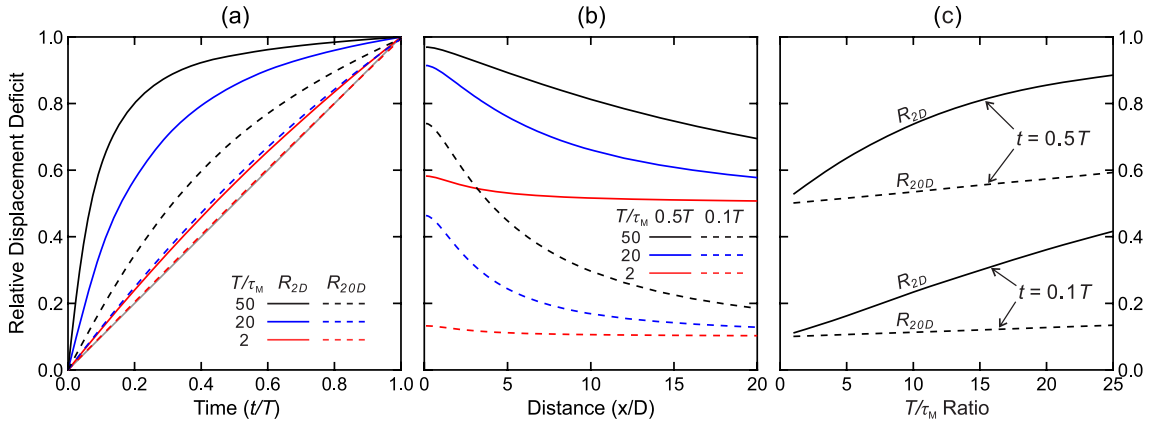

Figure 3. Relative Displacement Deficit (RDD) for a locked strike-slip fault (Equation 4). (a) Evolution of a near-field RDD (R_{2D}) and a far-field RDD (R_{20D}) in an earthquake cycle for three T/τ_M ratios. The gray line is from the elastic model (Figure 1a). (b) Variations in RDD with fault-normal distance at $t = 0.1T$ and $0.5T$ for the same three T/τ_M ratios as in (a). (c) R_{2D} and R_{20D} at the same two interseismic time points as in (b) for a wide range of T/τ_M ratios.

For a strike-slip fault that can be represented by the model in Figure 1d, a better metric of seismic readiness is RDD R_x, defined as

$$R_x(t) = \frac{U(x,t)}{U(x,T)} \tag{4}$$

It is the displacement at time t since the last earthquake at location x as a fraction of the final displacement at the end of the cycle. Obviously, the classical slip deficit is $S = U_o R_\infty(t)$ (in our specific numerical model, $R_\infty = R_{50D}$). $U(x,T)$, given by Equation 1 and shown in Figures 1c and 1f, is independent of T/τ_M and therefore is a good common reference.

For three selected T/τ_M ratios, Figure 3a shows the evolution of R_{2D} and R_{20D} in an earthquake cycle, and Figure 3b shows the spatial distribution of R_x at $t = 0.1T$ and $0.5T$. Even though $U(0,T) = 0$, Text S1 shows that RDD is a continuous and smooth function of x at the fault trace, and as $x \to 0$, $R_x(t) \to \Gamma_o(t)/\Gamma_o(T)$. The near-fault behavior of $R_x(t)$ makes the near-field RDD such as R_{1D} or R_{2D} a good representation of the strain energy accrued since the last earthquake. The reason why RDD is preferred over Γ_o is that it can be derived at any distance from the fault (Figure 3b). The near-field and far-field RDDs together characterize the deformation evolution of the larger system.

Figure 3c illustrates how R_{2D} and R_{20D} for a given t depend on T/τ_M. For very small T/τ_M ratios, $R_x U_o \approx R_\infty U_o = S$, and it is valid to use the elastic model. For a large T/τ_M such as 20, R_{2D} is already 85% at $t = 0.5T$, indicating that the fault is much more ready to fail than portrayed by a 50% slip deficit.

The RDD is based on a 2-D model and works better for long faults, although near-field RDD values are less affected by the 2-D assumption. In Figure S3, we display "type curves" similar to those in Figure 3a for a large range of T/τ_M values and a number of selected x values. To estimate the RDD from Figure S3 for a given time since the last earthquake, one needs the knowledge of rigidity and viscosity (and hence τ_M), in addition to the commonly used fault parameters such as V_o, T, and D.

3. Real-World Implications

3.1. Large Strike-Slip Faults

The models shown in Figure 1 can often be directly compared with real observations around large strike-slip faults. The Global Navigation Satellite Systems (GNSS) observations around two long-recurrence strike-slip faults in China from M. Wang & Shen (2020) are shown in Figure 4.

The >1,500 km long left-lateral Altyn Tagh Fault (ATF) exhibits along-strike variations in recurrence behavior, with the eastern part experiencing less frequent seismic rupture (Shao et al., 2018; Yuan et al., 2018).

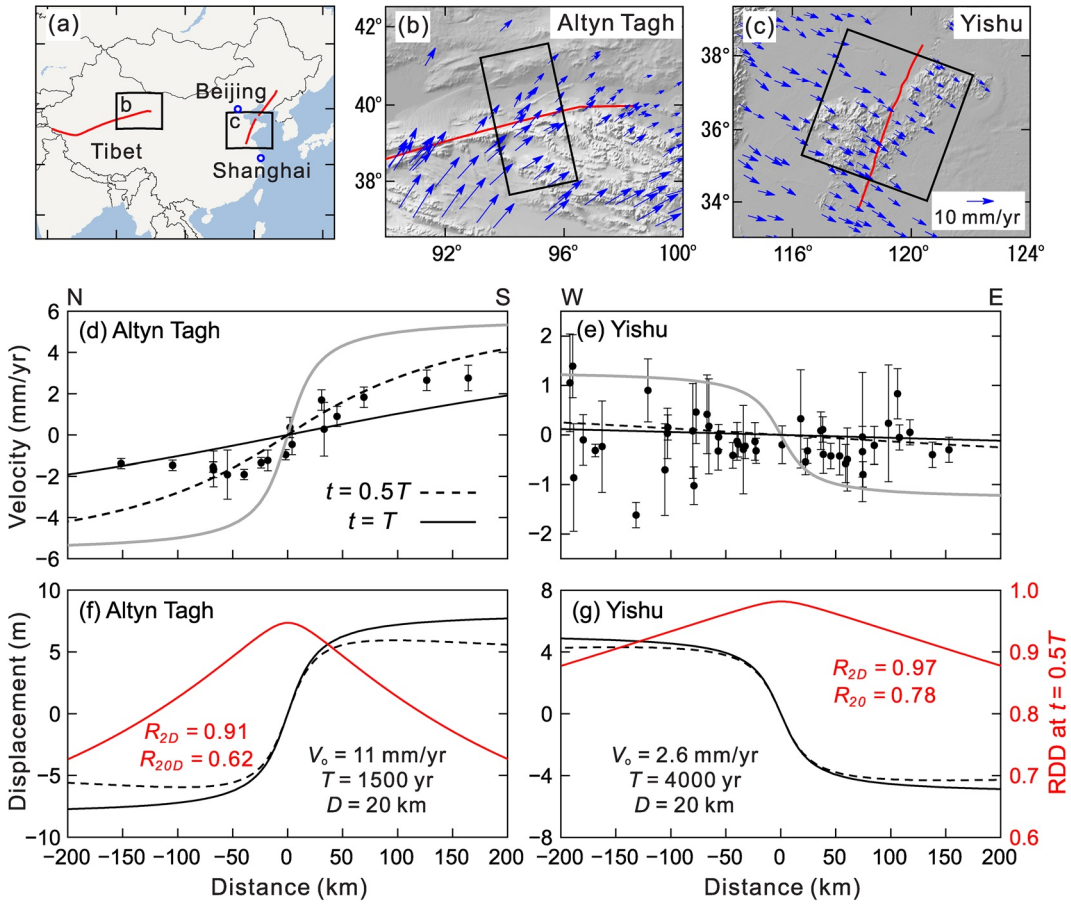

Figure 4. Observed and model-predicted interseismic deformation around two large strike-slip faults in China. The GNSS data and their one standard deviation error bars are from M. Wang and Shen (2020). τ_M = 50 years in the viscoelastic models (black curves, line style defined in (d)). (a) Map of China showing the locations of the two faults and map areas of (b) and (c). (b) and (c) Study areas of the Altyn Tagh Fault and Yishu Fault. GNSS data within the black rectangle are projected to a fault-normal profile shown in (d) and (e). (d) and (e) Fault-parallel component of GNSS velocities with respect to the fault trace in comparison with model results. Model parameters are shown in (f) and (g). The gray curve is from the elastic dislocation model (Figure 1a). (f) and (g) Displacements from the same viscoelastic models as in (d) and (e), respectively, and RDD at $t = 0.5T$ (red).

We pick the same fault-normal corridor as in Li et al. (2018) (Figure 4b) in the eastern part. The fault-parallel component of the GNSS velocities from this corridor is shown in Figure 4d. Here T is estimated to be ~1,500 years (Shao et al., 2018), and V_o from various geological studies ranges between 7.0–17.8 mm/yr (Y. Chen et al., 2012, 2013; Mériaux et al., 2005; Xu et al., 2005; Zhang et al., 2007). The elastic model (Figure 1a), with an average V_o = 11 mm/yr and a reasonable locking depth such as D = 20 km, is far from explaining the GNSS data (Figure 4d). It is not known when this segment last ruptured. Assuming we are presently somewhere between the mid-interseismic and late-interseismic stages, the viscoelastic model (Figure 1d) is more consistent with the observations (Figure 4d), although an exact fit cannot be obtained due to the simplicity of the model. If so, a large near-field RDD has been accumulated at present, evincing ample elastic strain energy for seismic rupture (Figure 4f).

For the right-lateral Yishu fault (Figure 4c), values of V_o = 2.6 mm/yr and T = 4,000 years are consistent with estimates from geological studies (Jiang et al., 2017). This fault produced the Tancheng earthquake in 1688, which is erroneously labeled as having a magnitude of 8.5 in the literature. More realistic parameters, especially the observed short rupture length, yield a moment magnitude (M_w) of about 7.5 (Zhu et al., 2020). Its geodetic signature today is very small and can be ignored in this discussion. If we assume that the fault is at the mid-interseismic to late-interseismic stage of its cycle of much larger earthquakes, the viscoelastic

model is much more compatible with the GNSS observations than is the elastic model (Figure 4e). Similar to the ATF, the model implies a large near-field RDD (Figure 4g).

There are other long-recurrence strike-slip faults that show very slow strain rates but probably have accumulated much energy to produce a large rupture. One example is the Garlock Fault in California which has an estimated V_o of 5–14 mm/yr and an average T of about 1,000 years (Dawnson et al., 2003; Dolan et al., 2016; Ganev et al., 2012; Madden Madugo et al., 2012). It is late in its earthquake cycle, and geodetic deformation rates appear to be very small (Chuang & Johnson, 2011; Rittase et al., 2014; Shen & Liu, 2020). A quantitative interpretation of the geodetic data would require detailed corrections for the effects of other nearby faults and is beyond the scope of this study, but it is worth pointing out that the low rate of deformation is compatible with a high near-field RDD.

3.2. Other Faults

Except for large strike-slip faults that are not strongly affected by other nearby faults, quantitative comparisons with actual observations would require addressing many other structural and kinematic details not included in the simple models discussed in this study. However, the fundamental concept illustrated by the simple models can help us understand first-order patterns of many observations.

Modeling interseismic deformation at subduction zones requires a realistic model structure and, in most cases, three-dimensional models (K. Wang et al., 2012). But the simple thrust model in Figure S1d is still qualitatively useful. The margin-normal geodetic contractile strain rates at the Cascadia subduction zone are generally less than 0.1×10^{-6}/yr (e.g., McCaffery et al., 2007). In comparison, at similar distances from the trench, the rates at the Nankai subduction zone are typically two or three times as high (Sagiya et al., 2000). Cascadia shares a similar subduction rate with Nankai and a similar thermal regime that controls the seismogenic depth of the megathrust, but its recurrence interval of megathrust earthquakes is longer by a factor of 5 and the last event (in 1700) preceded those at Nankai (in 1944 and 1946) by about 250 years (K. Wang, 2000). The present low rate of deformation at Cascadia is mostly a consequence of its being at a late stage of a relatively long interseismic period and does not imply lower likelihood than Nankai for a pending great earthquake.

The Longmenshan Fault in south-central China exhibits oblique-thrust motion with $V_o \approx 3$ mm/yr (Ma et al., 2005) and, $T \approx 4{,}000$ years (Burchfiel et al., 2008). In 2006, extremely low geodetic strain rates observed in this area led the Chinese geodetic community to conclude that this part of the Longmenshan Fault would not produce a large earthquake in the near future (Q.-F. Chen & K. Wang, 2010; Research Group of the China Earthquake Administration, 2007). But the fault ruptured in 2008 and caused the devastating $M_w = 7.9$ Wenchuan earthquake. The simple models in Figures 1d and S1d cannot quantitatively simulate the interseismic deformation before the Wenchuan earthquake because of the complex kinematics of the Longmenshan Fault and the "contamination" of the GNSS observations caused by neighboring fault systems (M. Wang & Shen, 2020). However, on the basis of what is learned from these models, we can argue that the pre-earthquake low strain rates are entirely consistent with the fault's being at the end of its very long interseismic period. Geodetic observations could not detect the large elastic strain already stored in the crust that was looming over the local population.

3.3. Recurrence Irregularity

The constant T assumed in the above discussion is for mathematical convenience, but it is not a necessary condition for the main physical process demonstrated by the model results. Given τ_M, even if T is not a constant, as long as the average recurrence interval of recent earthquakes is long, the behavior of the fault is still well represented by the models of high T/τ_M shown in Figures 2 and 3. Suppose we were at the stage $t = 0.5T$ of the ATF and wished to speculate the time of the next earthquake without the requirement that it must be at $t = T$. At this stage, RDD ≥ 91% within $2D$ of the fault (Figure 4f). Because failure stress can fluctuate from earthquake to earthquake due to spatiotemporal heterogeneities in fault structure and pore fluid pressure and due to perturbation by nearby earthquakes or other tectonic events, an earthquake may occur before R_{2D} reaches 100%. It may even occur when R_{2D} slightly exceeds 91%, that is, anytime soon.

Therefore, the acquisition of a high near-field RDD early on in the interseismic period combined with the natural randomness in failure stress should give rise to wide fluctuations in temporal spacing between successive earthquakes. This helps explain why faults with infrequent rupture exhibit greater variability in recurrence behavior than faults with frequent rupture (Berryman et al., 2012). At the Cascadia subduction zone that is characterized by infrequent but giant ($M_w \sim 9$) earthquakes, the recurrence interval is much more irregular (Atwater & Hemphill-Haley, 1997; Goldfinger et al., 2017) than at the Nankai subduction zone that is characterized by more frequent $M_w \sim 8$–8.5 earthquakes (Ando, 1975). These two subduction zones have similar convergence rates, but in general, more frequent rupture tends to be associated with faster V_o.

4. Conclusions

Using a simple earthquake cycle model, we clarify the implications of interseismic geodetic observations to the evaluation of earthquake potential of locked active faults in a viscoelastic Earth. These measurements only constrain the rate of deformation but not the strain energy already stored around a fault for the next earthquake. Given viscosity, if the earthquake recurrence interval is long, most of the energy for the next earthquake is accumulated in the early part of the interseismic period, represented by a high value of near-field RDD, and deformation rates decrease to a minimum toward the end of the period. The observed low rates of deformation do not imply low likelihood of a large earthquake. On the contrary, in some situations, a lower rate may imply greater immediacy of the next earthquake. Jointly interpreting geodetic data with paleoseismic and historical constraints in the viscoelastic framework will prove to be the most informative approach.

Data Availability Statement

No new data are used in this work. GNSS data displayed in Figure 4 are available through M. Wang & Shen (2020).

Acknowledgments
Funding for this study includes NSERC Discovery Grants RGPIN-2016-03738 to K. Wang and 2017-04029 to E. Nissen. This is Geological Survey of Canada contribution 20200646.

References

Ando, M. (1975). Source mechanisms and tectonic significance of historical earthquakes along the Nankai Trough, Japan. *Tectonophysics*, *27*(2), 119–140. https://doi.org/10.1016/0040-1951(75)90102-X

Atwater, B. F., & Hemphill-Haley, E. (1997). Recurrence intervals for great earthquakes of the past 3,500 years at Northeastern Willapa Bay, Washington. In *United States Geolological Survey Professional Paper 1576* (pp. 108).

Berryman, K. R., Cochran, U. A., Clark, K. J., Biasi, G. P., Langridge, R. M., & Villamor, P. (2012). Major earthquakes occur regularly on an isolated plate boundary fault. *Science*, *336*(6089), 1690–1693. https://doi.org/10.1126/science.1218959

Burchfiel, B. C., Royden, L. H., van der Hilst, R. D., Hager, B. H., Chen, Z., King, R. W., et al. (2008). A geological and geophysical context for the Wenchuan earthquake of 12 May 2008, Sichuan, People's Republic of China. *Geological Society of America Today*, *18*, 4–11. https://doi.org/10.1130/GSATG18A.1

Chen, Q.-F., & Wang, K. (2010). The 2008 Wenchuan earthquake and earthquake prediction in China. *Bulletin of the Seismological Society of America*, *100*(5B), 2840–2857. https://doi.org/10.1785/0120090314

Chen, Y., Li, S.-H., & Li, B. (2012). Slip rate of the Aksay segment of Altyn Tagh Fault revealed by OSL dating of river terraces. *Quaternary Geochronology*, *10*, 291–299. https://doi.org/10.1016/j.quageo.2012.04.012

Chen, Y., Li, S.-H., Sun, J., & Fu, B. (2013). OSL dating of offset streams across the Altyn Tagh Fault: Channel deflection, loess deposition and implication for the slip rate. *Tectonophysics*, *594*, 182–194. https://doi.org/10.1016/j.tecto.2013.04.002

Chuang, R. Y., & Johnson, K. M. (2011). Reconciling geologic and geodetic model fault slip-rate discrepancies in Southern California: Consideration of nonsteady mantle flow and lower crustal fault creep. *Geology*, *39*(7), 627–630. https://doi.org/10.1130/G32120.1

Dawson, T. E., McGill, S. F., & Rockwell, T. K. (2003). Irregular recurrence of paleoearthquakes along the central Garlock fault near El Paso Peaks, California. *Journal of Geophysical Research*, *108*(B7). https://doi.org/10.1029/2001JB001744

Dolan, J. F., McAuliffe, L. J., Rhodes, E. J., McGill, S. F., & Zinke, R. (2016). Extreme multi-millennial slip rate variations on the Garlock fault, California: Strain super-cycles, potentially time-variable fault strength, and implications for system-level earthquake occurrence. *Earth and Planetary Science Letters*, *446*, 123–136. https://doi.org/10.1016/j.epsl.2016.04.011

Ganev, P. N., Dolan, J. F., McGill, S. F., & Frankel, K. L. (2012). Constancy of geologic slip rate along the central Garlock fault: Implications for strain accumulation and release in southern California. *Geophysical Journal International*, *190*(2), 745–760. https://doi.org/10.1111/j.1365-246X.2012.05494.x

Goldfinger, C., Galer, S., Beeson, J., Hamilton, T., Black, B., Romsos, C., et al. (2017). The importance of site selection, sediment supply, and hydrodynamics: A case study of submarine paleoseismology on the northern Cascadia margin, Washington USA. *Marine Geology*, *384*, 4–46. https://doi.org/10.1016/j.margeo.2016.06.008

Hearn, E. H., & Thatcher, W. R. (2015). Reconciling viscoelastic models of postseismic and interseismic deformation: Effects of viscous shear zones and finite length ruptures. *Journal of Geophysical Research: Solid Earth*, *120*(4), 2794–2819. https://doi.org/10.1002/2014JB011361

Jiang, W., Zhang, J., Han, Z., Tian, T., Jiao, Q., Wang, X., & Jiang, H. (2017). Characteristic slip of strong earthquakes along the Yishu fault zone in east China evidenced by offset landforms. *Tectonics*, *36*(10), 1947–1965. https://doi.org/10.1002/2016TC004363

Johnson, K. M. (2013). Slip rates and off-fault deformation in Southern California inferred from GPS data and models. *Journal of Geophysical Research: Solid Earth*, *118*, 5643–5664. https://doi.org/10.1002/jgrb.50365

Li, Y., Shan, X., Qu, C., Liu, Y., & Han, N. (2018). Crustal deformation of the Altyn Tagh fault based on GPS. *Journal of Geophysical Research: Solid Earth*, *123*, 10309–10322. https://doi.org/10.1029/2018JB015814

Ma, B. Q., Su, G., & Hou, Z. H. (2005). Late Quaternary slip rate in the central part of the Longmenshan Fault zone from terrace deformation along the Minjiang River (in Chinese with English abstract). *Seismology and Geology*, *27*, 234–242.

Madden Madugo, C., Dolan, J. F., & Hartleb, R. D. (2012). New paleoearthquake ages from the western Garlock fault: Implications for regional earthquake occurrence in southern California. *Bulletin of the Seismological Society of America*, *102*(6), 2282–2299. https://doi.org/10.1785/0120110310

McCaffrey, R., Qamar, A. I., King, R. W., Wells, R., Khazaradze, G., Williams, C. A., et al. (2007). Fault locking, block rotation and crustal deformation in the Pacific Northwest. *Geophysical Journal International*, *169*, 1315–1340. https://doi.org/10.1111/j.1365-246x.2007.03371.x

Meade, B. J., Klinger, Y., & Hetland, E. A. (2013). Inference of multiple earthquake-cycle relaxation timescales from irregular geodetic sampling of interseismic deformation. *Bulletin of the Seismological Society of America*, *103*, 2824–2835. https://doi.org/10.1785/0120130006

Mériaux, A.-S., Tapponnier, P., Ryerson, F. J., Xiwei, X., King, G., Van der Woerd, J., et al. (2005). The Aksay segment of the northern Altyn Tagh fault: Tectonic geomorphology, landscape evolution, and Holocene slip rate. *Journal of Geophysical Research*, *110*(B4). https://doi.org/10.1029/2004JB003210

Nur, A., & Mavko, G. (1974). Postseismic viscoelastic rebound. *Science*, *183*(4121), 204–206. https://doi.org/10.1126/science.183.4121.204

Research Group of the China Earthquake Administration (2007). *Researches on earthquake risk regions and losses prediction of China continent from 2006 to 2020* (pp. 296). Seismological Press. (in Chinese).

Rittase, W. M., Kirby, E., McDonald, E., Walker, J. D., Gosse, J., Spencer, J. Q. G., & Herrs, A. J. (2014). Temporal variations in Holocene slip rate along the central Garlock fault, Pilot Knob Valley, California. *Lithosphere*, *6*(1), 48–58. https://doi.org/10.1130/L286.1

Sagiya, T., Miyazaki, S. i., & Tada, T. (2000). Continuous GPS array and present-day crustal deformation of Japan. *Pure and Applied Geophysics*, *157*, 2303–2322. https://doi.org/10.1007/PL0002250710.1007/978-3-0348-7695-7_26

Savage, J. C. (1983). A dislocation model of strain accumulation and release at a subduction zone. *Journal of Geophysical Research*, *88*(B6), 4984–4996. https://doi.org/10.1029/JB088iB06p04984

Savage, J. C., & Burford, R. O. (1973). Geodetic determination of relative plate motion in central California. *Journal of Geophysical Research*, *78*, 832–845. https://doi.org/10.1029/JB078i005p00832

Savage, J. C., & Prescott, W. H. (1978). Asthenosphere readjustment and the earthquake cycle. *Journal of Geophysical Research*, *83*(B7), 3369–3376. https://doi.org/10.1029/JB083iB07p03369

Shao, Y., Liu-Zeng, J., Oskin, M. E., Elliott, A. J., Wang, P., Zhang, J., et al. (2018). Paleoseismic Investigation of the Aksay Restraining Double Bend, Altyn Tagh Fault, and Its Implication for Barrier-Breaching Ruptures. *Journal of Geophysical Research: Solid Earth*, *123*(5), 4307–4330. https://doi.org/10.1029/2017JB015397

Shen, Z. K., & Liu, Z. (2020). Integration of GPS and InSAR data for resolving 3-dimensional crustal deformation. *Earth and Space Science*, *7*(4), e2019EA001036. https://doi.org/10.1029/2019EA001036

Shimazaki, K., & Nakata, T. (1980). Time-predictable recurrence model for large earthquakes. *Geophysical Research Letters*, *7*, 279–282. https://doi.org/10.1029/GL007i004p00279

Takeuchi, C. S., & Fialko, Y. (2012). Dynamic models of interseismic deformation and stress transfer from plate motion to continental transform faults. *Journal of Geophysical Research*, *117*, B05403. https://doi.org/10.1029/2011JB009056

Wang, K. (2000). Stress-strain 'paradox', plate coupling, and forearc seismicity at the Cascadia and Nankai subduction zones. *Tectonophysics*, *319*, 321–338. https://doi.org/10.1016/s0040-1951(99)00301-7

Wang, K., Hu, Y., & He, J. (2012). Deformation cycles of subduction earthquakes in a viscoelastic Earth. *Nature*, *484*(7394), 327–332. https://doi.org/10.1038/nature11032

Wang, M., & Shen, Z. K. (2020). Present-day crustal deformation of continental China derived from GPS and its tectonic implications. *Journal of Geophysical Research: Solid Earth*, *125*, e2019JB018774. https://doi.org/10.1029/2019JB018774

Xu, X., Wang, F., Zheng, R., Chen, W., Ma, W., Yu, G., & Ryerson, F. J. (2005). Late Quaternary sinistral slip rate along the Altyn Tagh. *Science in China, Series D: Earth Sciences*, *48*(3), 384. https://doi.org/10.1360/02yd0436

Yuan, Z., Liu-Zeng, J., Wang, W., Weldon, R. J., II, Oskin, M. E., Shao, Y., et al. (2018). A 6000-year-long paleoseismologic record of earthquakes along the Xorkoli section of the Altyn Tagh fault, China. *Earth and Planetary Science Letters*, *497*, 193–203. https://doi.org/10.1016/j.epsl.2018.06.008

Zhang, P.-Z., Molnar, P., & Xu, X. (2007). Late Quaternary and present-day rates of slip along the Altyn Tagh Fault, northern margin of the Tibetan Plateau. *Tectonics*, *26*(5), a–n. https://doi.org/10.1029/2006TC002014

Zhu, Y., Wang, K., & He, J. (2020). Effects of earthquake recurrence on localization of interseismic deformation around locked strike-slip faults. *Journal of Geophysical Research: Solid Earth*, *125*(8), e2020JB019817. https://doi.org/10.1029/2020JB019817